J. Electrochem. Sci. Eng. **15(5)** (2025) 2789; http://dx.doi.org/10.5599/jese.2789

Open Access : : ISSN 1847-9286
https://pub.iapchem.org/ojs/index.php/JESE

Original scientific paper

An electrochemical sensing platform based on ZnO-nanostructured modified glassy carbon electrode for sensitive hydroxylamine detection

Muhammad Abdel Hasan Shallal[1] and Hayfaa A. Mubarak[2,✉]

[1]*Department of Chemistry, College of Sciences, University of Dhi Qar, Iraq*
[2]*Chemical Engineering Department, College of Engineering, University of Babylon, Iraq*
Corresponding author: ✉haifaadnan_81@uobabylon.edu.iq

Received: May 6, 2025; Accepted: June 10, 2025; Published: August 2, 2025

Abstract

Background and purpose: Hydroxylamine is a reducing agent widely used in pharmacology and industry. The respiratory system, skin, eyes, and other mucous membranes are all irritated. Therefore, while researching biological industrial processes, quantitative HXA detection is crucial. Experimental approach: This study uses ZnO nanostructures on the glassy carbon electrode (GCE) surface to develop a sensitive electrochemical sensor for hydroxylamine (HXA). The drop-casting method was used to modify the sensor. Key results: The manufactured ZnO/GCE sensor showed outstanding catalytic performance for the electrooxidation of HXA. Using differential pulse voltammetry with a low limit of detection of 0.3 µM in the range of 0.5 to 470.0 µM, the ZnO/GCE demonstrated strong electrocatalytic performances toward HXA. Furthermore, in the detection of HXA, the ZnO/GCE demonstrated satisfactory repeatability and stability.

Keywords

Electrochemical sensor; differential pulse voltammetry; environmental pollutants; water sample

Introduction

Hydroxylamine (NH_2OH, HXA) is a key step in the nitrogen cycle and nitrous oxide generation process. Furthermore, HXA is a reducing agent that is widely used in pharmacology and industry. The respiratory system, skin, eyes, and other mucous membranes are all irritated. Given that HXA is a mutagen, using excessive amounts of it can be harmful to humans, animals, and plants. To ensure the safety of local marine species, government regulations were established for the quantity of HXA in the waste stream, which should be maintained at a low ppm level [1]. Therefore, while researching biological industrial processes, quantitative HXA detection is crucial. Ion chromatography [2], spectrophotometry [3], gas chromatography [4], biamperometry [5] and capillary electrophoresis [6] were among the methods used in reports to identify lower HXA. However, the afore

mentioned methods have more detection limits, less precision, expensive equipment, more steps in the sample preparation process, longer analysis times, and skilled specialists. Consequently, the development of techniques with increased sensitivity and dependability will be crucial [7].

In comparison to older methods, electrochemical methods are simpler, more sensitive, offer excellent reproducibility, provide faster analytical times, and are less costly [8,9].

A form of non-graphitic carbon known as glassy carbon (GC) emerges from the pyrolysis of specific polymeric precursors. Its internal architecture consists of distinct, curved graphene fragments, reminiscent of imperfect fullerene-linked nanoparticles, that intertwine randomly to form a dense carbon network [10]. When GC is synthesized at temperatures above 2000 °C, these curved sheets organize into stacked, ribbon-like graphite structures, and our analyses have even revealed polyhedral graphite crystals within commercial samples [10]. Thanks to its exceptional hardness, imperviousness, chemical inertness and high electrical conductivity, GC is widely employed as an electrode material in electroanalytical applications [11]. Moreover, its presumed inert surface makes it an ideal support for depositing powdered catalysts to evaluate their performance in various electrochemical reactions [12].

However, it is extremely challenging to get precise measurements of analytes due to the relatively weak response signal of typical sensors toward analyte detection. Therefore, electrochemical sensors are changed with different materials to increase the response signal of the analyte measurement [13].

Compared to bulk materials of the same composition, nanomaterials exhibit distinct physicochemical characteristics, such as high reactivity, ultra-small size, and a large surface area to mass ratio. The prospective applications of nanomaterials in various industries are determined by their special qualities or appealing traits [14].

Semiconductor metal oxides have long been recognized as critical nanostructured materials for applications in high-performance electronics, energy conversion and storage and environmental cleanup [15]. Among these, zinc oxide (ZnO) stands out for its unique combination of properties. As a II–VI semiconductor, ZnO exhibits bonding characteristics between purely covalent and purely ionic materials. Its notable attributes, including excellent mechanical and thermal stability at room temperature and a high exciton binding energy of 60 meV, have positioned it as a leading candidate for use in devices for electronics, laser systems, and optoelectronics [16].

Beyond these uses, ZnO's inherent piezoelectric and pyroelectric behaviours make it suitable for roles in photocatalysis, energy harvesting, sensing technologies, and even hydrogen production [16]. Its rigidity, hardness, and strong piezoelectric coefficient are also widely employed in advanced ceramics. Moreover, ZnO's low toxicity, biodegradability, and compatibility with biological systems have spurred its integration into biomedical devices and environmentally friendly technologies [16].

At the nanoscale, ZnO materials draw special attention due to their enhanced functionalities in electronic, photonic, and optical applications. In particular, ZnO nanostructures are ideal for fabricating highly sensitive sensors and biosensors, thanks to their wide band gap, substantial exciton binding energy, chemical and photochemical stability, non-toxicity, biocompatibility, and excellent charge-transport properties [17,18].

To detect HXA in aqueous buffer solutions, the current study set out to design, fabricate, and describe the preparation and suitability of a ZnO nanostructure modified GCE (ZnO/GCE). It then evaluated the modified electrode's analytical performance in quantifying HXA. Eventually, the actual samples were analysed to use the newly suggested electrochemical sensor to detect HXA.

Experimental

Reagents and solutions

Hydroxylamine hydrochloride (HXA) was obtained from Sigma-Aldrich and employed without further modification. To prepare a 0.01 M HXA solution, the appropriate mass of HXA was dissolved in distilled water and then quantitatively transferred into a 100 mL volumetric flask, which was brought to volume with additional Milli-Q water. The resulting stock was stored at 4 °C until use. For experiments requiring lower concentrations, this stock was serially diluted using phosphate buffer.

A 0.1 M phosphate buffer solution (PB) was formulated by mixing equal volumes of 0.1 M sodium dihydrogen phosphate (NaH_2PO_4) and 0.1 M disodium hydrogen phosphate (Na_2HPO_4), and the pH was fine-tuned to the desired value with either dilute hydrochloric acid or sodium hydroxide. All other chemicals were of analytical-reagent grade and were used without further purification. Every solution was prepared using water that had been deionized and double-distilled.

Apparatus

For the electrochemical determination, an Autolab potentiostat/galvanostat 312 N (Switzerland) was utilized. The three electrochemical cell systems were composed of a GCE (either unmodified or modified), a saturated calomel reference electrode (SCE) and a Pt wire auxiliary electrode.

Synthesis of ZnO nanostructures

With a few minor adjustments, the hydrothermal technique was used to create ZnO nanostructures, as previously described by Liang *et al.* [19]. To create ZnO nanostructures, 70 mL of deionized water was mixed with 0.297 g of $Zn(NO_3)_2{\times}6H_2O$ (1 mmol) and 0.120 g of urea (2 mmol), and the mixture was stirred for 30 minutes at room temperature. The hydrothermal procedure was then carried out in a Teflon-lined stainless-steel autoclave. Precursors were cooked in an autoclave for six hours at 95 °C in an oven. To remove contaminants, the resulting precipitates were centrifuged for five minutes at 6000 rpm after being repeatedly washed with ethanol and deionized water. The collected precipitates were then calcined in a muffle furnace for two hours at 300 °C after being dried in air for fifteen hours at 70 °C. The FESEM image of synthesized nanostructure can be seen in Figure 1.

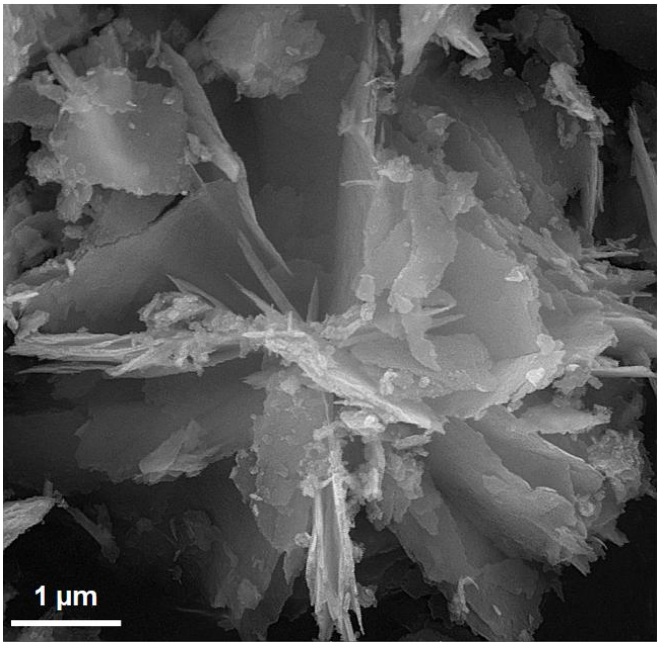

Figure 1. *FESEM image of ZnO nanostructures*

Preparation of the modified GCE

The GCE was polished using alumina slurry on a polishing cloth before the alteration procedure began. It was then thoroughly cleaned with water and allowed to air dry. Next, 0.5 mL of deionized water was mixed with 0.5 mg of ZnO nanostructures, and the mixture was homogenized for 20 min using ultrasonics. ZnO/GCE was then formed by drop-casting 3.0 µL of the well-dispersed solution onto the GCE surface using a micropipette and allowing it to dry at room temperature.

Real sample preparation

We used a variety of water samples, including drinking water and river water, as the actual samples in accordance with the research design. The water samples were then filtered three times before analysis. As a result, different amounts of HXA were added to the water samples, which were then analysed using the conventional addition method.

Results and discussion

Electrochemical properties of electrodes

The cyclic voltammetry (CV) was used to electrochemically characterize the ZnO/GCE in the presence of 3.0 mM $[Fe(CN)_6]^{3-/4-}$ redox couple (1:1, molar ratio) containing 0.1 M KCl (Figure 2). To find the electrochemical active surface areas (*A*), CV measurements were conducted on ZnO/GCE in $[Fe(CN)_6]^{3-/4-}$ solution at various scan rates between 10 and 400 mV s^{-1}. For the reversible electrode process, the Randles-Ševčik Equation (1) was used [20], which defines the peak current, I_p:

$$I_p = \pm(2.69\times10^5)n^{3/2}AD^{1/2}C\nu^{1/2} \quad [1]$$

C = 3.0 mM is the concentration of $K_3[Fe(CN)_6]$, D = 7.2×10^{-6} cm^2 s^{-1} is the diffusion coefficient, A / cm^2 is the electrode surface area, and n is the number of electrons engaged in the redox process (n = 1 for $K_3[Fe(CN)_6]$). The slope of the plot of I_{pa} *vs.* $\nu^{1/2}$ may then be used to calculate the electroactive area for ZnO/GCE (0.051 cm^2).

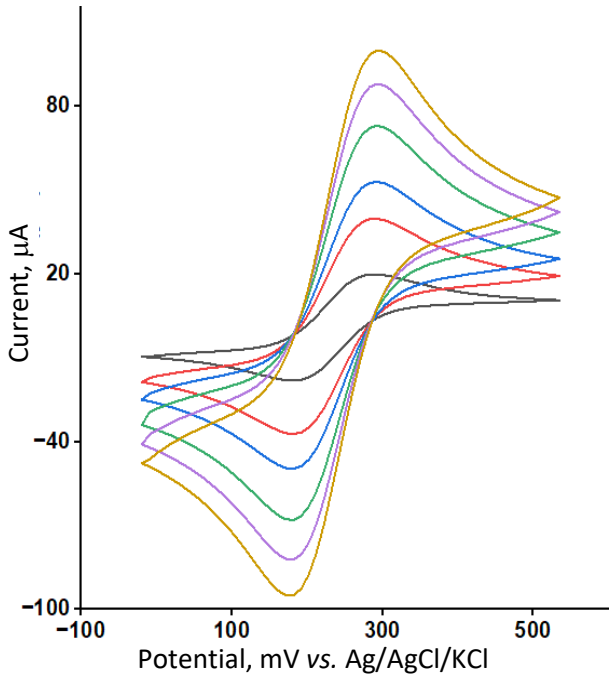

Figure 2. *CVs of ZnO /GCE in the presence of 3.0 mM $[Fe(CN)_6]^{3-/4-}$ at different scan rates (10 to 400 mV s^{-1})*

The same procedure was used with bare GCE and a 0.033 cm^2 electroactive area of bare GCE was obtained.

One important tool for figuring out the electron transport properties of the modified electrode is electrochemical impedance spectroscopy (EIS) using Nyquist plots (Figure 3). The features of the electrode interface may be described by the electrode surface electron transfer resistance, or R_{ct}, which is equal to the EIS semicircle diameter. A sizable semicircle with a diameter of around 800 Ω (R_{ct}) was visible at the bare GCE, indicating a notably poor electron transfer rate between the GCE and the electrochemical probe $[Fe(CN)_6]^{3-/4-}$. The R_{ct} decreased to 310 Ω when the ZnO nanostructures were added to the GCE. The figure illustrates the variations in impedance at the modified electrode, confirming the remarkable conductivity of ZnO nanostructures that accelerate electron transfer. The surface area characteristics and the synergistic effect of ZnO nanostructures on the $[Fe(CN)_6]^{3-/4-}$ electrochemical response were the causes of the obvious impedance variations.

The standard heterogeneous rate constant (k^0) for every electrode was also determined by EIS using Equation (2) [20]:

$$k^0 = RTF^2R_{ct}AC \quad [2]$$

where T is the standard temperature (298.15 K), F is the Faraday constant (96485 C mol^{-1}), R_{ct} / Ω is the electron transfer resistance, A / cm^2 is the electrode surface area, C is the concentration of the $[Fe(CN)_6]^{3-/4-}$ solution (1.0 mM), and k^0 / cm s^{-1}is the standard heterogeneous electron transfer rate constant. The ZnO/GCE and bare GCE yielded k^0 values of 1.5×10^{-2} and 3.8×10^{-2} cm s^{-1}, respectively. Given that the kinetic facility of the redox pair is measured by the k^0 values, a system with a high k^0 will reach equilibrium faster than a system with a low k^0, which will take longer in this scenario. Therefore, the k^0 with the ZnO/GCE sensor is higher than with ZnO/GCE > GCE, suggesting a quicker electron transfer compared to the bare electrode.

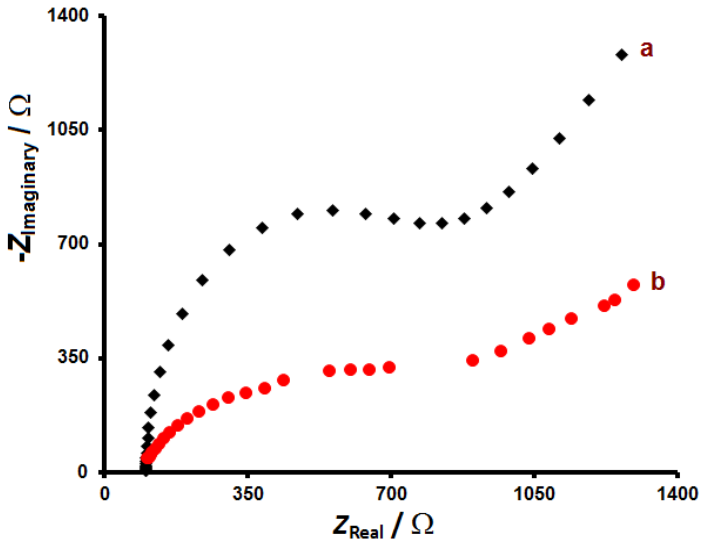

Figure 3. *Nyquist diagrams of bare GCE (a) and ZnO/GCE (b) in the buffer solution (pH 7.0) containing $K_3[Fe(CN)_6]$ (C = 3.0 mM)*

Electrochemical behaviour of hydroxylamine

This study examines the electrochemical behaviour of HXA at both modified and unmodified GCEs. For a 300.0 µM HXA in PBS, at the unmodified GCE and ZnO/GCE, CVs were measured at 50 mV s^{-1} (Figure 4). At the ZnO/GCE surface, the HXA current peak oxidation potential is 850 mV *vs.* SCE, which is about 160 mV more negative than that exhibited in the case of the unmodified GCE. When the oxidation peak currents for HXA at the unmodified GCE and ZnO/GCE are compared, the anodic peak current at the ZnO /GCE is enhanced by almost 5.6 to 12.1 µA due to the increased surface area and facilitated charge transfer kinetics.

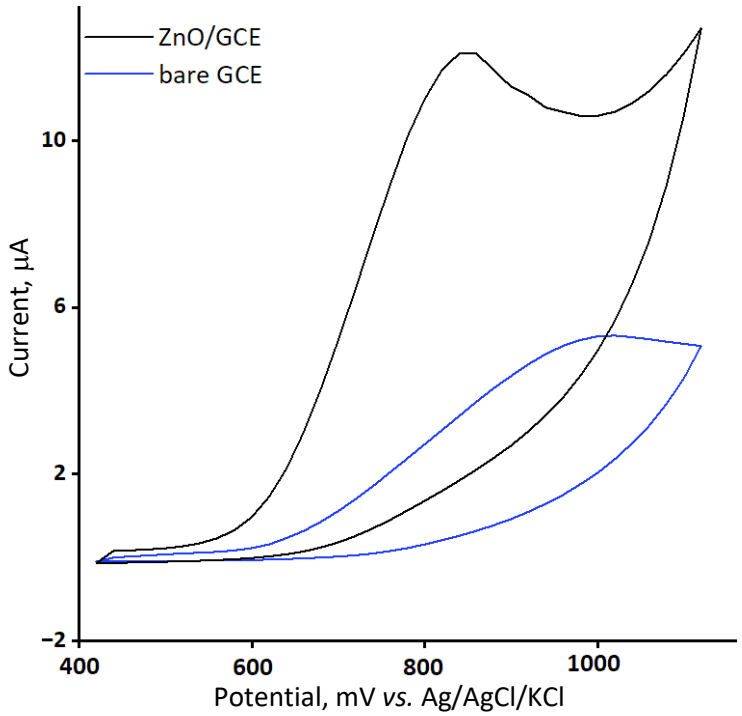

Figure 4. *CVs of bare GCE and ZnO /GCE in the presence of 300.0 µM HXA at a pH 7.0. The scan rate was 50 mV* s^{-1}

Effect of pH

Using PBS solutions, the effects of pH on the electrochemical behaviour of HXA were investigated in the pH range of 3.0 to 9.0 using DPV. It was discovered that when the pH of the solutions increases, the peak potential shifts toward less positive values, indicating that the proton is involved in the electrochemical process. The peak potential (E_p) and pH have a linear relationship, following the regression Equation (3):

$$E_p = -57.143\text{pH} + 1251.34 \quad R^2 = 0.9994 \qquad (3)$$

The equation's slope is around the Nernstian value of -59 mV, indicating that the oxidation of HXA involves an equal number of protons and electrons.

The oxidation peak current of HXA increases up to pH 7.0 and then decreases. As a result, the ideal pH for the electrochemical tests was determined to be 7.0.

Potential sweep rate effect

Linear sweep voltammetry (LSV) was employed to investigate the effect of scan rate on the oxidation peak current of HXA on the ZnO/GCE. Figure 5A illustrates that the peak current and scan rate are directly proportional, indicating that higher scan rates correspond to higher peak currents. Furthermore, as shown in Figure 5B, current is proportional to the square root of scan rate (ν) in the 10-300 mV s^{-1} range, which indicates a diffusion control of the HXA oxidation process. These findings also showed that increasing the scan rate resulted in a positive shift in the oxidation peak potential. Additionally, there are kinetic constraints at higher scan rates during the interaction between ZnO/GCE and HXA.

Tafel curves were plotted using data from rising portions, or Tafel regions, of the current-voltage curve obtained at 10 mV s^{-1}. The Tafel regions of current potential curves are influenced by the electron transfer kinetics of the electrode processes. The findings reveal a 0.14 V Tafel slope, indicating one electron rate-determining step (RDS) for the electron process with a charge transfer coefficient (α) of 0.58.

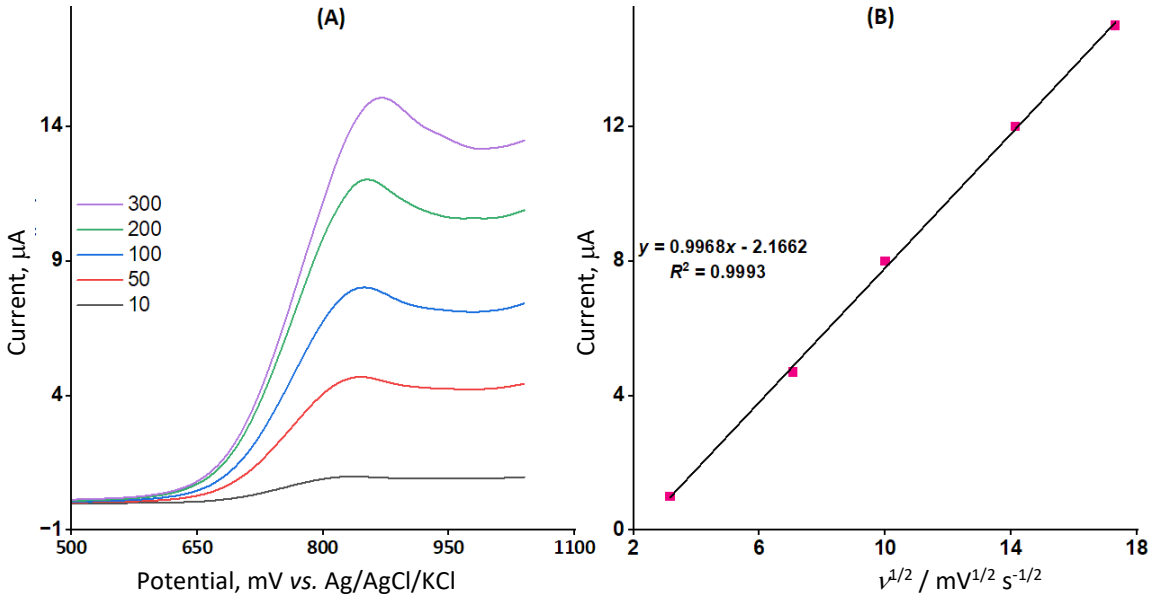

Figure 5. *(A) ZnO/GCE LSVs at different scan speeds in 0.1 M PB (pH 7.0) with 100.0 µM HXA, (B) peak currents plotted against* $\nu^{1/2}$

Chronoamperometric measurements

Chronoamperometric measurements of HXA were performed on the ZnO/GCE by holding the electrode potential at 900 mV *versus* Ag/AgCl (3.0 M KCl) and recording the current response upon successive additions of HXA in PBS, as illustrated in Figure 6A.

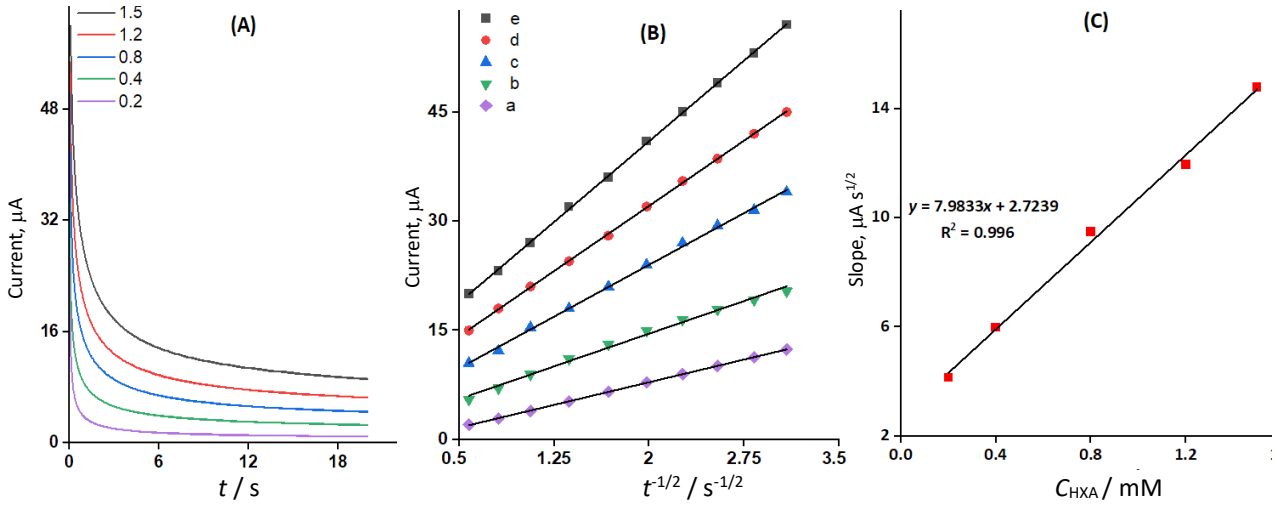

Figure 6. *(A) Chronoamperograms for various HXA concentrations (0.2 to 1.5 mM) at ZnO/GCE in 0.1 M PB (pH 7.0), (B)* I vs. $t^{-1/2}$ *plots derived from chronoamperograms (a- 0.2, b -0.4, c- 0.8, d - 1.2 and e - 1.5 mM) and (C) plot of the straight-line slopes versus the concentration of HXA*

Under conditions where mass transport of the electroactive species (here, HXA) governs the current, the Cottrell equation (4) describes the time-dependent decay of the chronoamperometric signal, with *D* representing the diffusion coefficient [20].

$$I = nFAD^{1/2}C_b\pi^{-1/2}t^{-1/2} \quad (4)$$

Here, D / cm^2 s^{-1}, n = 2 and C_b / mol cm^{-3} stand for the diffusion coefficient, number of electrons and bulk concentration, respectively. The best fits for different HXA concentrations were found using *I vs.* $t^{-1/2}$ test plots (Figure 6B). Plotting the resulting straight-line slopes against codeine concentrations was subsequently done (Figure 6C). *D* mean values were determined using the Cottrell equation and the resulting slope, and for HXA, they were 5.43×10^{-6} cm^2 s^{-1}.

Voltammetric determination of HXA

Under ideal experimental circumstances, an HXA calibration curve was obtained using DPV measurements. Figure 7A shows the usual DPVs for different HXA concentrations. A linear range of 0.5 to 470.0 µM was obtained with a HXA slope value of 0.0374 µA μM^{-1} (Figure 7B). The HXA limit of detection was 0.3 µM.

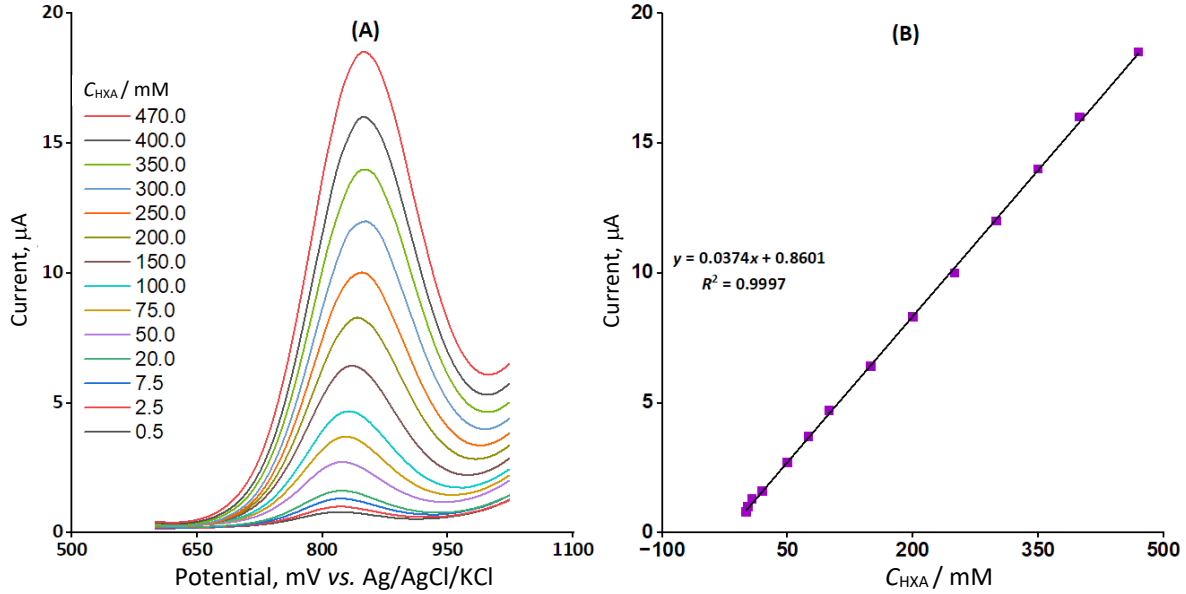

Figure 7. *(A) ZnO/GCE DPVs in 0.1 M PB (pH 7.0) with varying HXA concentrations. (B) Electrocatalytic peak current plotted against HXA concentration in the 0.5 to 470.0 µM range*

Sample analysis

HXA was measured in water samples at ZnO/GCE to demonstrate the practical application of the proposed approach. Each sample was handled in accordance with the voltammetric determination of section HXA. For every sample, five parallel determinations were made. The findings are shown in Table 1. The relative standard deviation (RSD) was less than 3.4 %, and the recoveries ranged from 96.7 to 104.0 %. The acquired findings demonstrate that the suggested approach is applicable to actual samples.

Table 1. *HXA measurement in water samples (n = 5)*

Sample	C_{HXA} / mM		Recovery, %	RSD, %
	Spiked	Found		
Drinking water	0	-	-	-
	5.0	4.9	98.0	2.2
	7.0	7.2	102.9	3.4
	9.0	8.8	97.8	1.9
	11.0	11.1	100.9	2.7
River water	0	-	-	-
	4.0	4.1	102.5	3.3
	6.0	5.8	96.7	2.1
	8.0	7.9	98.7	2.9
	10.0	10.4	104.0	3.0

Stability and repeatability

The long-term stability of ZnO/GCE was assessed during a three-week period. Based on this, the tests were conducted again after the modified electrode was stored in an environment for three

weeks and not used for three weeks. DPVs showed that the HXA oxidation peak potential remained unchanged, with the exception of a 2.2 % current drop when compared to the main reaction. DPVs were used to analyse the antifouling properties of the modified electrode with respect to HXA oxidation. At a scan rate of 50 mV s^{-1}, voltammograms were recorded in the presence of HXA after 15 possible cycles. The results revealed a 3.6 % drop in currents and no changes in peak potentials. According to the findings, using the modified ZnO/GCE reduces the impacts of HXA fouling while increasing sensitivity.

Conclusions

A new, ZnO nanostructured electrochemical sensor was prepared for the efficient determination of hydroxylamine. ZnO nanostructures were prepared with a one-pot synthesis procedure in essence, the ZnO nanostructure is a modifier for GCE that promotes mass transport, electrocatalysis, and electron transfer. In terms of sensitivity, the ZnO nanostructure enhanced the electrochemical reaction of HXA and significantly reduced the overvoltage. Additionally, ZnO/GCE was utilized to directly measure HXA in actual specimens without the need for treatments, yielding positive findings. This indicates that ZnO/GCE is a favourable electrode for on-site HXA detection.

References

[1] M. Chen, T. He, X. Liang, C. Wang, C. Zheng, Efficient transformation of hydroxylamine from wastewater after supplementation with sodium carbonate or calcium bicarbonate, *Ecotoxicology and Environmental Safety* **266** (2023) 115603. https://doi.org/10.1016/j.ecoenv.2023.115603

[2] A. M. Prokai, R. K. Ravichandran, Simultaneous analysis of hydroxylamine, N-methylhydroxylamine and N, N-dimethylhydroxylamine by ion chromatography, *Journal of Chromatography A* **667** (1994) 298-303. https://doi.org/10.1016/0021-9673(94)89079-X

[3] L. Dai, J. Xu, J. Lin, L. Wu, H. Cai, J. Zou, J. Ma, Iodometric spectrophotometric determination of peroxydisulfate in hydroxylamine-involved AOPs: 15 min or 15 s for oxidative coloration? *Chemosphere* **272** (2021) 128577. https://doi.org/10.1016/j.chemosphere.2020.128577

[4] J. A. Sagona, J. E. Dukett, H. A. Hawley, M. A. Mazurek, Sequential derivatization of polar organic compounds in cloud water using O-(2, 3, 4, 5, 6-pentafluorobenzyl) hydroxylamine hydrochloride, N, O-bis (trimethylsilyl) trifluoroacetamide, and gas-chromatography/mass spectrometry analysis, *Journal of Chromatography A* **1362** (2014) 16-24. https://doi.org/10.1016/j.chroma.2014.08.001

[5] C. Zhao, J. Song, Flow-injection biamperometry for direct determination of hydroxylamine at two pretreated platinum electrodes, *Analytica Chimica Acta* **434** (2001) 261-267. https://doi.org/10.1016/S0003-2670(01)00846-7.

[6] S. Zorbas-Seifried, M. Jakupec, N. V. Kukushkin, M. Groessl, C. G. Hartinger, O. Semenova, B. K. Keppler, Reversion of structure-activity relationships of antitumor platinum complexes by acetoxime but not hydroxylamine ligands, *Molecular pharmacology* **71** (2007) 357-365. https://doi.org/10.1124/mol.106.030726

[7] U. K. Deogratias, D. Jin, X. Zhang, N. A. H. Forde, G. Y. Bhrane, M. A. Jalloh, P. Wu, Double-edged effects and regulation mechanism of hydroxylamine in novel nitrogen removal processes: A comprehensive review, *Journal of Water Process Engineering* **69** (2025) 106826. https://doi.org/10.1016/j.jwpe.2024.106826

[8] Y. Xie, M. De Ras, J. Zhao, T. Liu, F. Lai, J. Hofkens, M.B. Roeffaers, Electrochemical reduction of nitrate to hydroxylamine on gold electrode, *Chemical Communications* **60** (2024) 10918-10921. https://doi.org/10.1039/d4cc03620d

[9] A. Ramesh, N. S. Gudipati, S. R. K. Vanjari, C. Subrahmanyam, High-performance amperometric detection of hydroxylamine on fluorine doped tin oxide electrode modified with $NiCo_2O_4$ nanoparticles, *Electrochimica Acta* **461** (2023) 142692. https://doi.org/10.1016/j.electacta.2023.142692

[10] P. Lakhera, V. Chaudhary, A. Jha, R. Singh, P. Kush, P. Kumar, Recent developments and fabrication of the different electrochemical biosensors based on modified screen printed and glassy carbon electrodes for the early diagnosis of diverse breast cancer biomarkers, *Materials Today Chemistry* **26** (2022) 101129. https://doi.org/10.1016/j.mtchem.2022.101129

[11] A. S. Murali, B. Saraswathyamma, High Performance Electrochemical analysis of Water Pollutant: Catechol Utilizing Mesoporous Fe_2O_3/NiO/CuO Composite Modified Glassy Carbon Electrode, *Ceramics International* **51(14)** (2025) 18492-18504. https://doi.org/10.1016/j.ceramint.2025.02.029

[12] A. S. Murali, U. Rajaji, K. Yusuf, B. Saraswathyamma, T.Y. Liu, High efficiency electrochemical sensing of 4-Nitrotoulene: A new approach utilizing MoO_3/CeO_2 integrated glassy carbon electrode, *Microchemical Journal* **212** (2025) 113473. https://doi.org/10.1016/j.microc.2025.113473

[13] Y. Wang, H. Xiong, X. Zhang, Y. Ye, S. Wang, Nitromethane biosensor based on four heme proteins modified glassy carbon electrodes, *Journal of Electroanalytical Chemistry* **674** (2012) 17-22. https://doi.org/10.1016/j.jelechem.2012.04.004

[14] M. Sher, A. Faheem, W. Asghar, S. Cinti, Nano-engineered screen-printed electrodes: A dynamic tool for detection of viruses, *Trends in Analytical Chemistry* **143** (2021) 116374. https://doi.org/10.1016/j.trac.2021.116374

[15] S. Zhang, M. Tan, S. Du, W. Leng, D. Wu, Bas e-metal oxide semiconductor electrodes for PPCP degradation: Ti-doped α-Fe_2O_3 for sulfosalicylic acid oxidation as an example, *Chemosphere* **313** (2023) 137354. https://doi.org/10.1016/j.chemosphere.2022.137354

[16] M. Yadav, S. Choudhari, P. Kumar, P. Ram, Zinc oxide nano-flowers synthesized via a hydrothermal approach for electrochemical performance as a supercapacitor electrode, *Journal of the Indian Chemical Society* **102** (2025) 101667. https://doi.org/10.1016/j.jics.2025.101667

[17] K. Mariappan, S. P. Sivaji, H. Y. Hsu, T. W. Chen, S. M. Chen, M. C. Yu, T. W. Chiu, Three-dimensional flower-like strontium doped zinc oxide decorated with carbon black modified glassy carbon electrode for the detection of strychnine, *Journal of Alloys and Compounds* **1009** (2024) 176825. https://doi.org/10.1016/j.jallcom.2024.176825

[18] A. Yildirim, M. Maral, B. T. Zaman, A. Bozoglu, C. Demir, S. Bakırdere, A. Erdem, Graphene oxide-zinc oxide nanocomposite modified disposable electrodes for detection of uric acid in fetal bovine serum, *Journal of Electroanalytical Chemistry* **965** (2024) 118345. https://doi.org/10.1016/j.jelechem.2024.118345

[19] Y. Liang, N. Guo, L. Li, R. Li, G. Ji, S. Gan, Fabrication of porous 3D flower-like Ag/ZnO heterostructure composites with enhanced photocatalytic performance, *Applied Surface Science* **332** (2015) 32-39. https://doi.org/10.1016/j.apsusc.2015.01.116

[20] A. J. Bard and L. R. Faulkner, *Electrochemical methods fundamentals and applications*, 2nd edition, Wiley, New York, USA (2001). ISBN: 978-1-118-31280-3